PIER B

Compact Wideband Antenna Array with DGS-Based Metamaterial for Efficient Smartphone Communication and SAR Reduction

Amany A. Megahed[1], Amr H. Hussein[2], Ahmed Jamal Abdullah Al-Gburi[3,*], and Rania Hamdy Elabd[1,4]

[1]*Electronic and Communication Department*
Higher Institute of Engineering and Technology in New Damietta, Damietta 34517, Egypt
[2]*Electronics and Electrical Communications Engineering Department*
Faculty of Engineering, Tanta University, Egypt
[3]*Centre for Telecommunication Research & Innovation (CeTRI)*
Fakulti Teknologi dan Kejuruteraan Elektronik dan Komputer (FTKEK)
Universiti Teknikal Malaysia Melaka (UTeM), Malacca, Malaysia
[4]*Electronics and Communications Engineering Department*
Faculty of Engineering, Horus University Egypt, New Damietta, Egypt

ABSTRACT: This study investigates a high-gain, miniaturized antenna array featuring semicircular Defected Ground Structures (DGSs) based metamaterial designed for wideband smartphone applications. The antenna array, measuring $49 \times 25 \, \text{mm}^2$, is constructed on an FR4 substrate with a dielectric constant of 4.3 and a thickness of 1.6 mm. The design incorporates two orthogonal antennas, each with a U-shaped radiating patch and a semicircular DGS to control bandwidth and reduce size. A T-shaped stub is positioned at the center of the U-shaped radiating area, with a star-shaped element attached to the leg of the T-shaped stub to enable wideband operation. The antenna demonstrates strong S_{11} performance, achieving approximately $-38 \, \text{dB}$ at 5.8 GHz and $-42 \, \text{dB}$ at 8.1 GHz, making it ideal for Sub-6 GHz and C-band applications. The proposed antenna array operates across a frequency range from 4 GHz to beyond 10 GHz, reaching a peak gain of 11 dBi and an efficiency of 95%. A time-domain analysis was conducted to verify radiation efficiency, and the specific absorption rate (SAR) is approximately 0.0475 for 1 g of tissue and 0.0101 for 10 g of tissue at 4.5 GHz, confirming the array's suitability for wideband smartphone devices within the target frequency band. The simulated and experimental results of the proposed antenna array show excellent agreement.

1. INTRODUCTION

Mobile telecommunications facilities are becoming increasingly widespread worldwide. People often use their phones close to their heads. As wireless mobile services expand globally, mobile phone manufacturers must consider the interactions between human bodies and mobile devices. On one hand, the electromagnetic waves emitted by the antenna are partially absorbed by the human skull. On the other hand, the presence of a human head affects several characteristics of mobile phone antennas, such as radiation efficiency, bandwidth, return loss, and radiation pattern. For the fifth-generation (5G) connectivity, the majority of academic institutions have focused on achieving high throughput and high data rates at a low cost [1–5]. The 5G communication systems are expected to offer data rates 1000 times faster than the fourth-generation (4G) communication systems [1]. The 5G Radio Access Networks (RANs) are anticipated to manage multiple 5G bands concurrently, in addition to a variety of frequencies [6]. Numerous metrics have been developed by the ITU-R to assess the demand for the spectrum necessary for international mobile telephony (IMT). The

ITU-R recently completed nearly all of the research required to meet the 2020 demand for this spectrum [7]. The proposed antenna is capable of covering the ITU n79 (4.4–5 GHz) and C-band (4–8 GHz) 5G frequency bands. Extensive studies indicate that the lower frequency range will provide significantly superior coverage for contemporary wireless communications. 5G communication is expected to offer greater data speeds and larger coverage areas with outdoor-to-indoor network coverage by utilizing frequency bands lower than 6 GHz [8]. Printed antenna technology is widely used in many well-performing sub-6 GHz antenna designs described in the literature. Modern technologies have produced extremely small and highly efficient antennas. The most popular type of antenna in this category is printed microstrip slot antenna [9–13]. Slot antennas are applicable to a wide range of applications, including 4G LTE, WLAN, Bluetooth, and WiMAX. In addition to the uses mentioned above, slot antennas are extensively utilized in wireless 5G applications, most of which now involve mobile terminal devices. The proposed rectangular slot antenna design is primarily aimed at sub-6 GHz 5G applications for phones and portable devices.

* Corresponding author: Ahmed Jamal Abdullah Al-Gburi (ahmedjamal@ieee.org).

The literature describes various slot antenna design methods, including transformer triple-band slot antenna [9], cross-formed slit coupler antenna [14], round patch antenna with asymmetric open slits [15], octagonal slit antenna with U-shaped strips for ultra-wideband (UWB) applications [16], monopole patch with a square slit and L-shaped strips [17], and C-shaped coupled-fed antenna with an L-shaped monopole slot featuring orthogonal polarization [18]. Additionally, a broad slot antenna with hypothetical resonances is also noted [19]. Other identified antenna types include user-hand effect F-shaped slotted multiple-input multiple-output (MIMO) antenna [20], dual monopole antennas with rectangular etched slots and a T-shaped stub [21], an elliptical patch with an elliptical slot and dipole feed [22], an antenna with complementary split-ring resonator (CSRR) slots, a meandered coplanar waveguide (CPW) feed [23], and U-shaped slot antennas.

However, the comparatively high gain, enhanced efficiency, and compact size of printed slot antenna designs remain a challenge. Several disadvantages of slot antennas for 5G applications in the sub-6 GHz region are documented in [24, 25]. These disadvantages include large slot sizes, narrow impedance bandwidth, low gain, low efficiency, etc. Because 5G portable devices have limited space, the antenna must be integrated with the dielectric back cover of the phone. This makes low-profile antennas essential for 5G applications. Specifically, the total thickness of the antenna at 3.3 GHz should be around 1 mm [26].

The specific absorption rate (SAR), a well-defined metric, is used to calculate the amount of energy absorbed by human tissue. SAR limits are safety regulations set by the Federal Communications Commission (FCC) to protect consumers from radio-frequency radiation. According to IEEE standards for SAR [27], it is the time derivative of the excess energy absorbed (or dissipated) by a mass contained in a volume element with a specific density (1/2). The SAR limit for any 10 g of tissue is 2 W/kg, according to IEEE C95.1:2005 [27]. The recommendations of the International Committee on Non-Ionizing Radiation Safety and this limit are comparable [28–30].

This study illustrates the architecture and implementation of a high-gain compact antenna array with semicircular defected ground structure (DGS)-based metamaterials for wideband smartphone applications. A transmission line provides the feed for the U-shaped radiating patch. The antenna can be miniaturized by reducing its size and adjusting the bandwidth through the semicircular DGS etched beneath the radiating patch. The antenna array design incorporates two orthogonal antennas. The U-shaped configuration of the single radiating patch is intended to minimize the antenna area and manage bandwidth using the semicircular DGS. To enable wideband operation, a T-shaped stub is attached at the center of the U-shaped radiating area, with a star-shaped element placed in the center of the T-shaped stub's leg. The proposed array can operate between 4 GHz and over 10 GHz, achieving a maximum gain of 11 dBi and a maximum efficiency of 95%. The antenna functioned as intended during simulations when the dielectric rear cover and human head-hand model were included. A safe use value of 0.0101 W/kg for SAR at 4.5 GHz, with superior

efficiency and radiation patterns, has been established by the investigation. Excellent agreement is found between the measurements and models.

2. PROPOSED ANTENNA ELEMENT STRUCTURE

In this section, highly efficient and compact designs for wideband antenna structures are introduced. The proposed antenna structures based semicircular slot DGS is designed on an FR4 substrate of thickness $h = 1.6$ mm, dielectric constant/relative permittivity $\varepsilon_r = 4.5$, and loss tangent $\delta = 0.025$. The proposed radiating patch is intended to have a U-shape structure with a transmission line feed having a width L_2. Beneath the radiating patch, a semicircle-DGS is engraved to control the bandwidth and minimize the aspect of the antenna. A T-shaped stub construction is affixed in the centre of the U-shaped radiating area, and a star-shaped element is affixed in the centre of the leg of T-shaped stub to enable wide-band operation as presented in Figure 1. The sizes of the printed planned U-shaped antenna, which is DGS, are 21×21 mm^2.
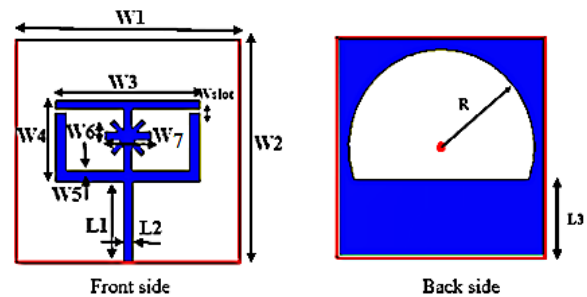

FIGURE 1. The modelled single element structure.

Figure 2 shows the procedure for making an antenna patch step-by-step. Initially, a rectangular radiating patch is modelled with the dimensions $W_3 \times W_4$. The sides of the rectangular patch are found using Equations (1) and (2) [31], and the matching reflection coefficient $|S_{11}|$ is plotted in Figure 2(b). As revealed in Figure 2(b), the bandwidth of the first stage extends from 3.8 GHz to 4.5 GHz.

$$W_3 = \frac{C}{4f_o\sqrt{\frac{\varepsilon_r+1}{2}}} \tag{1}$$

$$W_4 = \frac{C}{4f_o\sqrt{\varepsilon_{\text{eff}}}} \tag{2}$$

$$\varepsilon_{\text{eff}} = \frac{\varepsilon_r + 1}{2} + \frac{\varepsilon_r - 1}{2}\frac{1}{\sqrt{1 + 12\frac{h}{W_3}}} \tag{3}$$

In this case, h, ε_{eff}, C, and f_o stands for FR4 substrate's height, equivalent permittivity, (3×10^8 m/s) rapidity of light, and center frequency, correspondingly.

To improve impedance matching and attain resonance in the WB spectrum, a rectangular ring is constructed on the patch's surface, as seen in the second stage. Rectangular ring tends to create bandwidth responses between 3.8 GHz to 4.5 GHz and between 9 GHZ to 10 GHz, as seen in Figure 2(b). A plus sign
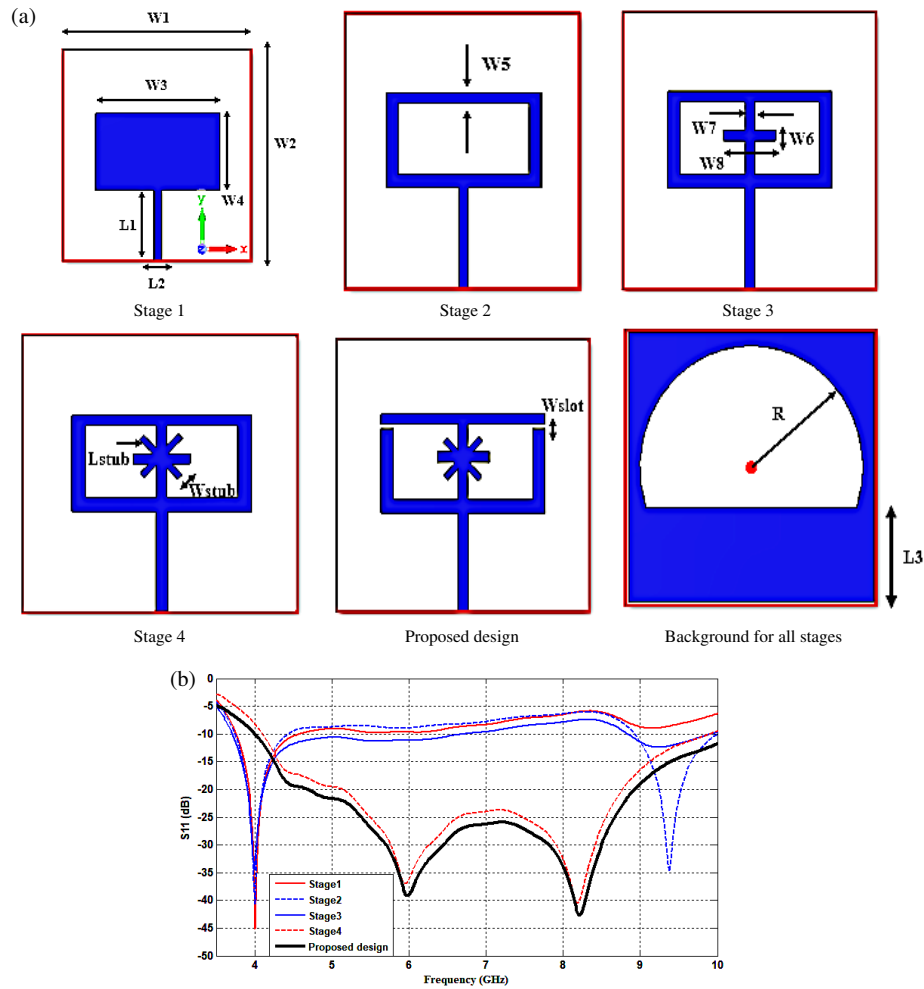
FIGURE 2. (a) Phases of the planned U-Shaped antenna's progressive design, and (b) reflection coefficient $|S_{11}|$ of different phases.

TABLE 1. Parameters of designed antennas in millimetres.

W_1	W_2	W_3	W_4	L_3
21	21	13.5	7.35	5.33
R	W_{slot}	L_{stub}	W_{stub}	W_5
9.5	0.3	4.1	0.5	0.8
W_6	W_7	L_1	L_2	
0.8	4.3	6	0.86	

FIGURE 3. Fabricated single element structure.

shaped stub was formed at the third step's center of the preceding phase, as shown in Figure 2. Figure 2 illustrates how adding a plus sign shaped stub frequently produces a WB response and improves impedance matching. Figure 2(b) displays the corresponding S_{11} from 3.8 GHz to 6 GHz and from 9 GHz to 10 GHz. Further, impedance matching is realized, as demonstrated in the suggested single antenna element, by making a cross sign shaped stub around the plus sign shaped stub in the fourth step. This tends to widen the bandwidth from 4.2 GHz to 9.8 GHz. For further enhancement, a slot is made in the top side of the rectangular ring in the proposed element. Figure 2(b) displays the corresponding S_{11} from 4 GHz to more than 10 GHz. The Computer Simulation Technology (CST) Microwave Stu-
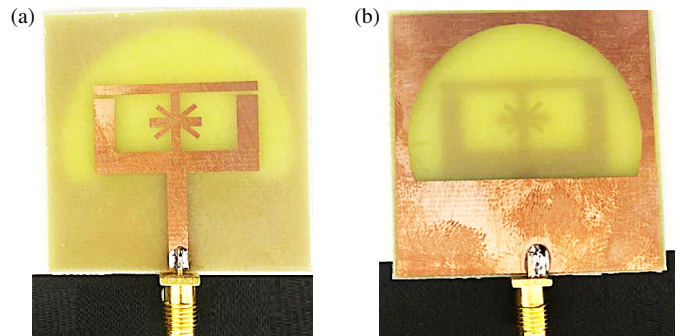
dio v2019 is applied to the scheme and virtual reality processes. The formal features of the radiator element are listed in Table 1. A single element is fabricated, and Figures 3(a) and (b) present a shot of the finished antenna buildings.

Figure 4(a) illustrates how the single element of proposed antenna is computer-generated by a 50-ohm proximity-coupled microstrip line. The Gain Transfer Method/Gain Comparison Method has been used to evaluate the gain of the planned antenna design in accordance with the IEEE standard test proce-
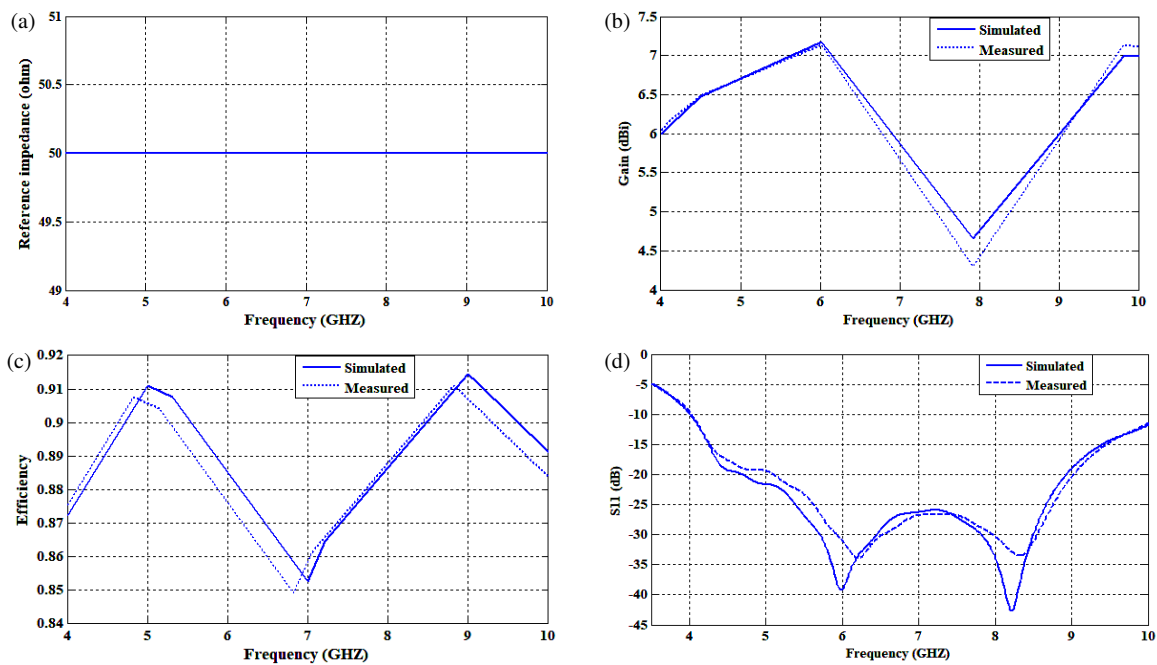
FIGURE 4. (a) Reference impedance of planned single antenna, (b) gain, (c) efficiency, and (d) simulated and measured S_{11}.
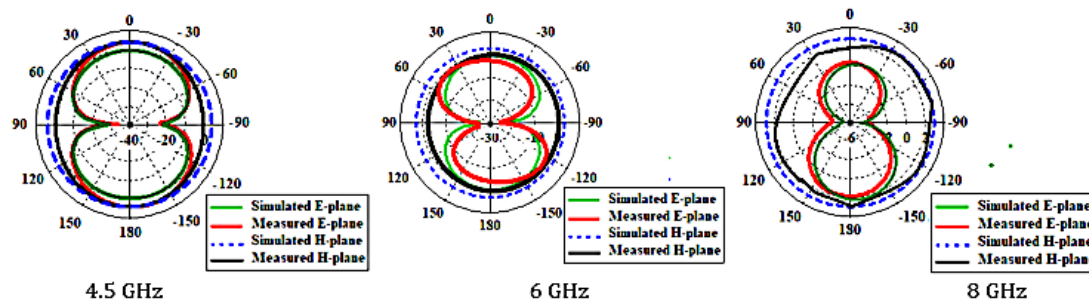

FIGURE 5. The measured and simulated 2D radiation patterns.

dure. The gain computation uses a single reference antenna that is located on an antenna positioner within an anechoic chamber, and it has a known gain. After that, the built prototype is oriented to face the direction of maximum radiation and to run parallel to the reference horn antenna. In order to calculate the gain of the planned antenna in relation to the reference antenna, we activated the S_{21} parameter during the measurement procedure using Vector Network Analyzer (VNA). The proposed antenna's realized peak gain is 7 dBi as displayed in Figure 4(b).

Since all antenna measurement tools are automated, the gain is determined prior to the directivity and reflection coefficient. The antenna's efficiency is computed last. According to the observed data, the constructed prototype radiates at a total efficiency of around 91%, which is similar to the outcomes of the simulations displayed in Figure 4(c). Figure 4(d) demonstrates the computer-generated and observed return loss of the planned single antenna. In Figure 4(d), the result indicates the computer-generated and measured reflection coefficient BW

($|S_{11}| < -10$ dB) from 4 GHz to more than 10 GHz, indicating 5G sub-6 GHz (4.5 GHz) and C-band (4 GHz to 8 GHz).

Figure 5 depicts the computer-generated and observed 2D radiation patterns of the proposed antenna at the desired frequencies of 4.5 GHz, 6 GHz, and 8 GHz. Co-polarization and cross-polarization plots are presented in the radiation pattern for both the E-plane and H-plane. It is clear that the observed and computer-generated patterns are closely matched. The slight discrepancies between the observed and computer-generated results may be due to inaccuracies during the manufacturing and soldering of the connectors. Additionally, the settings of the anechoic chamber, which may contain additional metal, can contribute to the variations in the measured S-parameters and radiation patterns.

Figure 6 displays the appropriate surface current distribution of the suggested antenna for 4.5 GHz, 6 GHz, and 8 GHz. The transmission feed line is where the most of the currents were found to be flowing. It is demonstrated that the currents are concentrated near the surface of the antenna. Therefore, the BW will be broadened as a result of these currents.
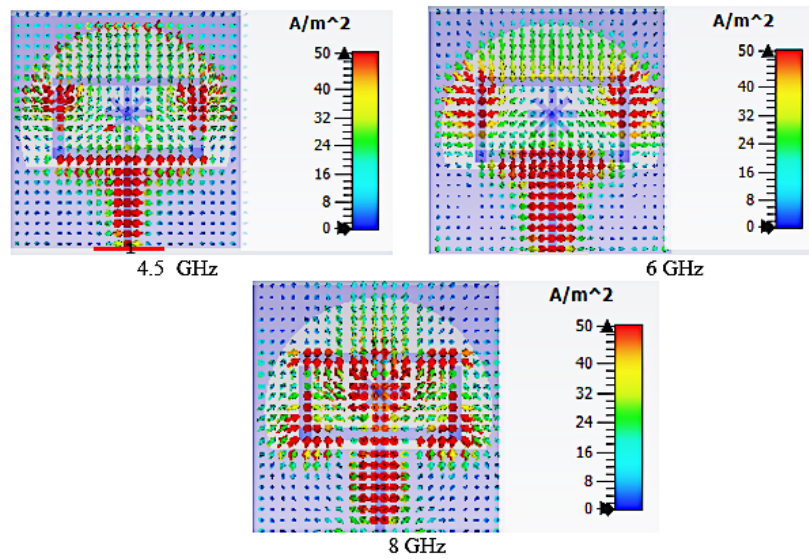
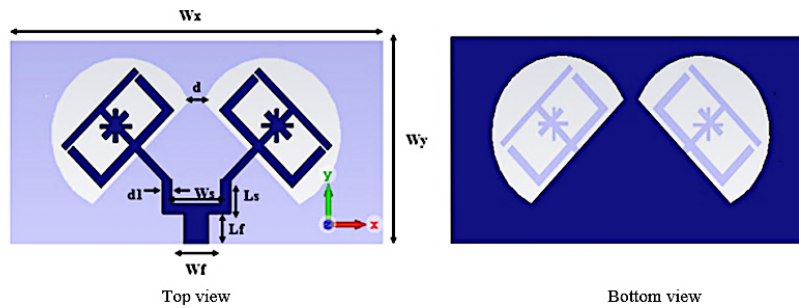**FIGURE 6**. Distribution of surface current in a single-element antenna.

Top view   Bottom view

FIGURE 7. The planned WB antenna array configuration's structural design. The modelled antenna array geometry.

3. ARRAY ANTENNA WITH DGS-BASED METAMATE-RIAL CONFIGURATION

The development of the orthogonal U-shaped antenna array with a semicircular DGS for operating frequencies ranging from 4 GHz to 10 GHz is shown in this section. The rationale behind the planned antenna array is to use two components from the single element in the preceding section by a 100-ohm proximity-coupled microstrip line that is 90° inclined relative to each other in order to broaden the BW and boost the gain. The planned antenna array is made on an FR4 substrate with a 0.025 loss tangent and dielectric constant 4.3, as shown in Figure 7. The antenna array is stimulated by means of a 50-ohm proximity-feed microstrip line, as shown in Figure 8(a). The geometric design aspects are explained in detail. The ideal design specifications are shown in Table 2. A simplified depiction of a wideband antenna's electrical behavior using lumped components such as resistors, capacitors, and inductors is called an equivalent circuit model. This method aids in the analysis and comprehension of the resonant behavior, impedance matching, and antenna performance. Wideband antennas are made to function across a wide range of frequencies. Wideband antennas have several resonances or a continuous response throughout a broad frequency range, in contrast to narrowband antennas that only have one resonance. To il-

TABLE 2. The ideal parameters for the planned antenna array (in millimetres).

d	1.86
d_1	1.3
W_x	49
W_y	25
L_f	3.8
W_s	6.4
W_f	3.2
L_s	4.09

lustrate this in a circuit that is comparable: Radiation losses and ohmic losses are represented by resistors (R); inductive effects brought on by current routes or antenna structures are represented by inductors (L); and capacitive coupling and energy storage are represented by capacitors (C). By combining these elements, the antenna's frequency-dependent impedance can be modeled.

An appropriate approximation aimed at a thin band antenna is LC resonant circuit. The entire wideband resonances of the UWB antenna are formed by the overlying resonant frequencies of a cascade of LC resonators that make up broadband antennas. Advanced Design System (ADS) program is employed to

TABLE 3. The component circuit's final findings.

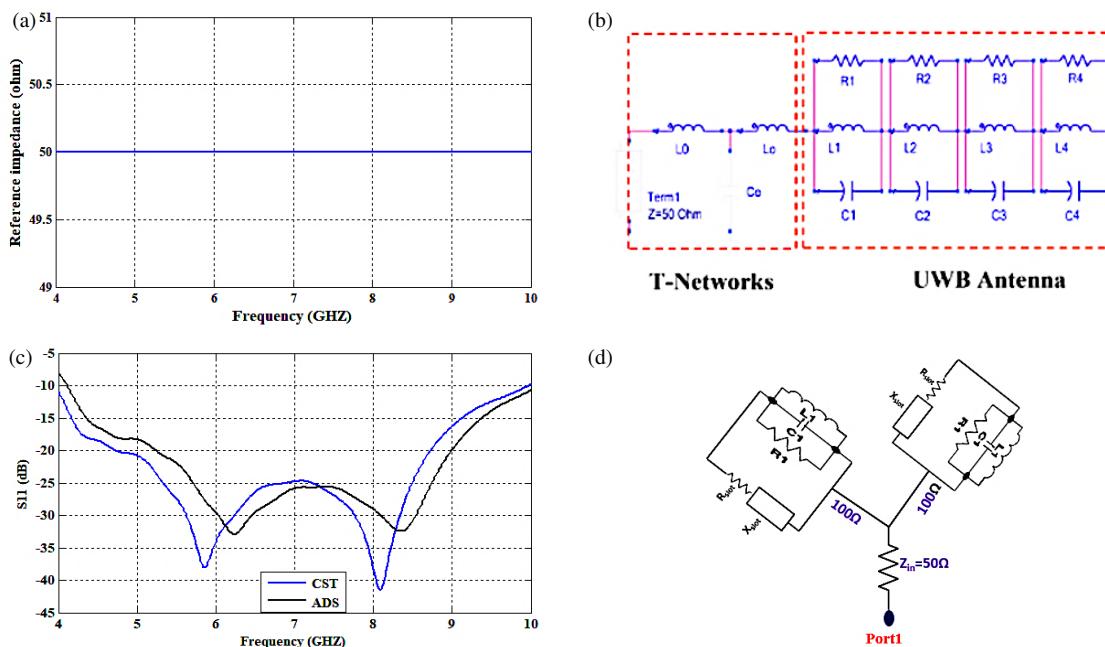| L_o	C_o	R_1	L_1	C_1	R_2	L_2
0.158 nH	0.085 pF	60.96 Ω	1.425 nH	1.89 pF	60.67 Ω	0.894 nH
R_3	L_3	C_3	R_4	L_4	C_4	C_2
42.84 Ω	0.098 nH	1.56 pF	59.19 Ω	0.163 nH	0.792 pF	0.79 pF

FIGURE 8. (a) Reference impedance of the planned antenna array, (b) wide band antenna equivalent circuit, (c) ADS and CST outcomes, and (d) planned antenna equivalent circuit.

design the circuit of the UWB antenna. The lumped element of the circuit is shown in Figure 8(b), and its components are listed in Table 3. The virtual reality results for the similar circuit and perfect simulation are contrasted, as shown in Figure 8(c). Equations (4) and (5) can be utilized to determine the Lo and Co components for the transmission line in the proposed antenna's equivalent circuit design [32]. Equations (6) and (7) are utilized to determine the inductance and capacitance for the lumped circuit components. After combining and adjusting the component values, the antenna equivalent circuit is drawn using ADS software. The obtained results for the total resonant frequencies between the CST and ADS programs are depicted in the figure as being in good agreement. The final circuit of WB antenna array is shown in Figure 8(d).

$$L_o = 100h \left(4\sqrt{\frac{W_f}{h}} - 4.21 \right) \qquad (4)$$

$$C_o = W_f \left[(9.5\varepsilon_r + 1.25)\frac{W_f}{h} + 5.2\varepsilon_r + 7 \right] \qquad (5)$$

$$L = \frac{img(Z_{11})}{2\pi f} \qquad (6)$$

$$C = \left[(2\pi f)^2 L \right]^{-1} \qquad (7)$$

In this case, W_f, h, ε_r stand for width of the feed, thickness of substrate, and dielectric constant, respectively.

After the antenna array is built, views of the completed antenna structures are shown in Figures 9(a) and (b). The computer-generated and observed reflection coefficient $|S_{11}|$ curves are shown in Figure 10(a). High agreement between the computer-generated and observed findings is shown by the outcomes, and the observed return loss BW ($|S_{11}| < -10$ dB) covers from 4 GHz to 10 GHz, showing C-band (4 GHz to 8 GHz)
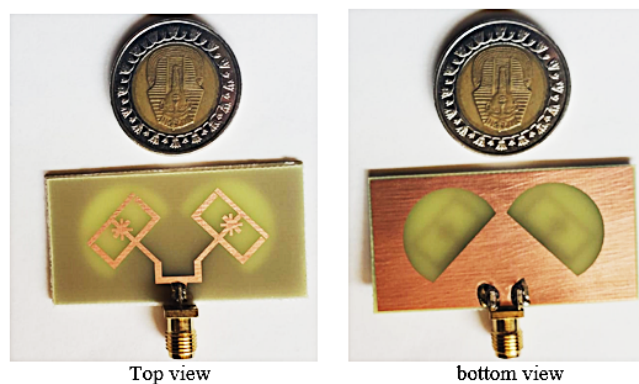

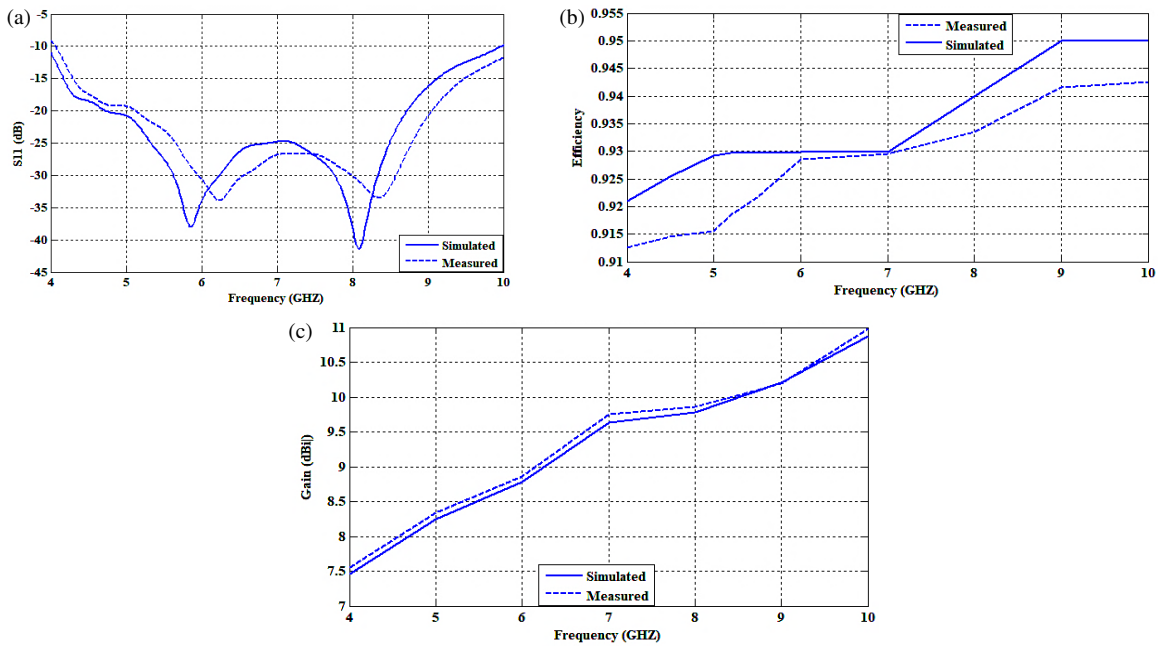| Top view | bottom view |

FIGURE 9. Fabricated antenna array.

FIGURE 10. Computer generated and observed values, (a) return loss, (b) efficiency and (c) gain.
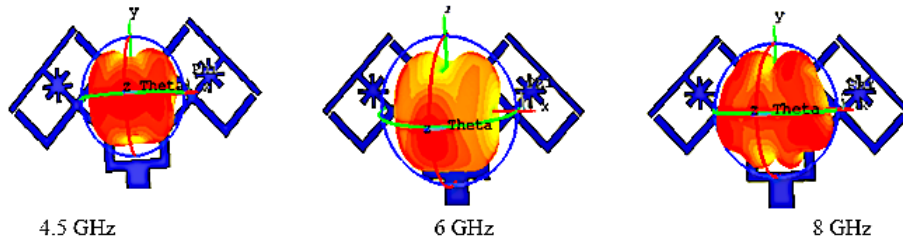

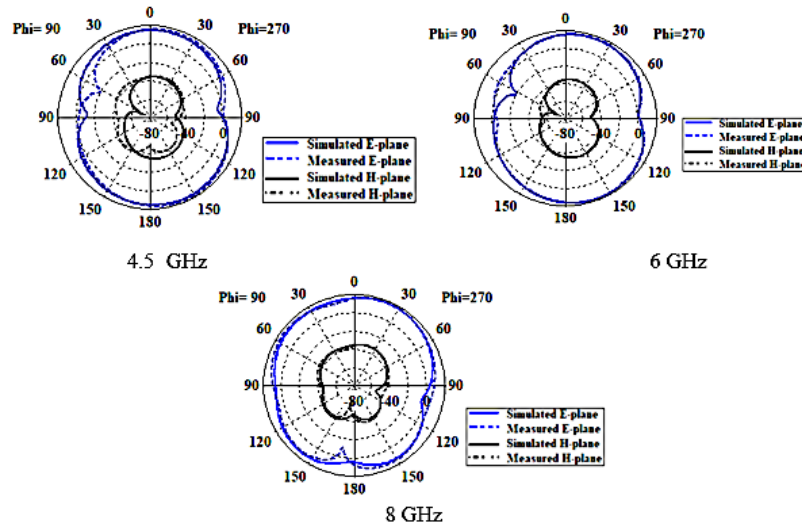**FIGURE 11**. 3D radiation design of planned array.

FIGURE 12. 2D radiation shape of planned array.

and 5G sub-6 GHz (4.5 GHz). Figures 10(b) and (c) show the gain and efficiency. The maximum efficiency and gain of the antenna are brought into being to be 95% and 11 dBi, respectively.

Figures 11 and 12 show the 3D and 2D radiation characteristics at frequencies of 4.5 GHz, 6 GHz, and 8 GHz, in that order. Both the computer-generated and observed radiation contours for the E and H planes are shown. The antenna exhibits the typ-
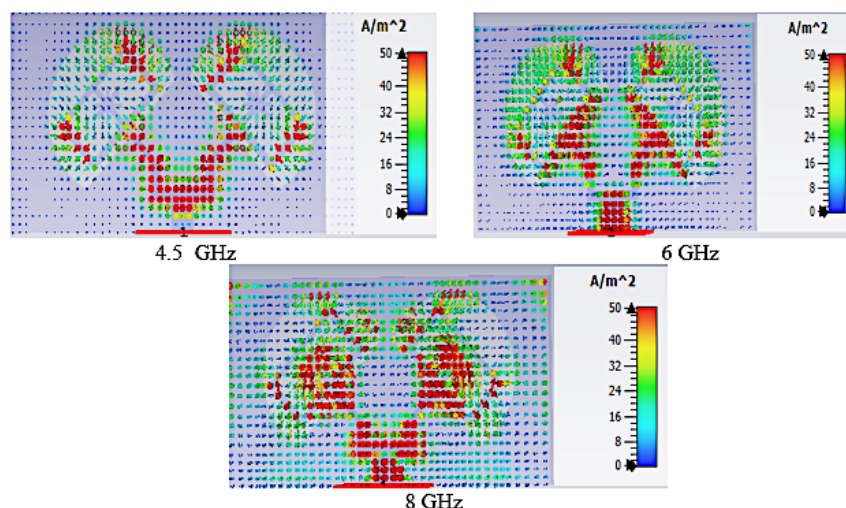
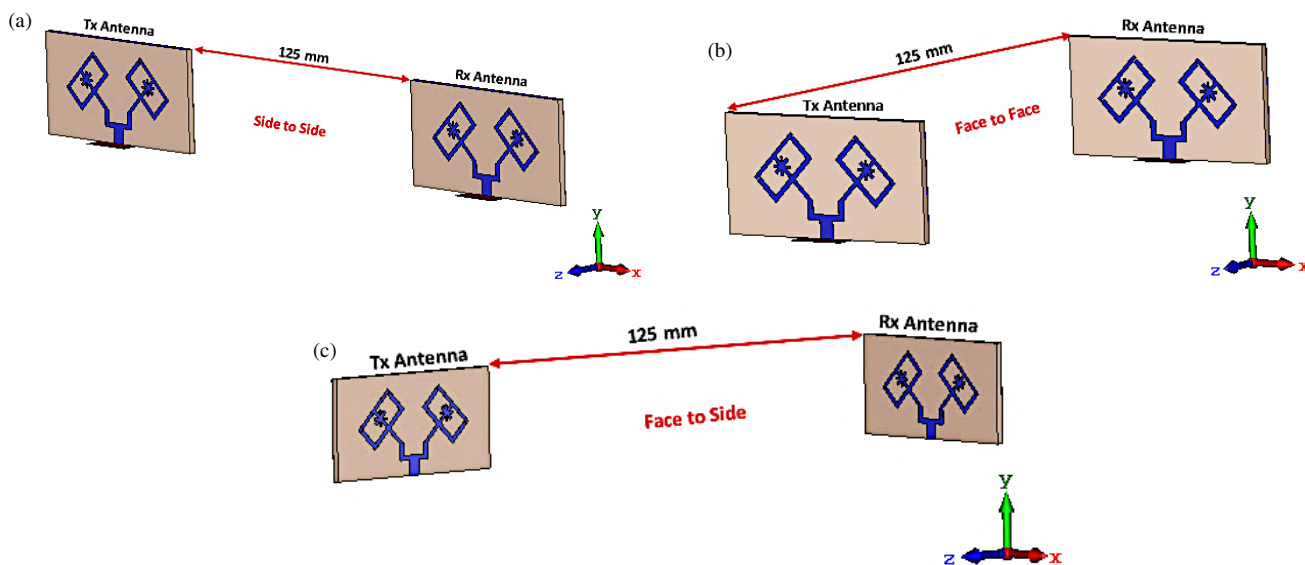**FIGURE 13**. Distribution of surface currents of planned array.

FIGURE 14. Pattern of time-domain analysis in dissimilar simulation setups.

ical monopole radiation characteristics. It is evident from the simulated results that radiation is emitted from the suggested antenna in all directions. The computer-generated and observed radiation forms accord fairly well. Figure 13 displays the appropriate surface current distribution of the suggested antenna for 4.5 GHz, 6 GHz, and 8 GHz. The transmission feed line is where the most of the currents were found to be flowing. It is demonstrated that the currents are concentrated near the surface of the antenna. Therefore, the BW will be broadened as a result of these currents.

4. EVALUATION OF THE ANTENNA'S TIME-DOMAIN PERFORMANCE

The presentation of the antenna in the time domain is thoroughly examined, covering group delay, S_{21} phase, and forward transmission coefficient (S_{21}). Figure 14 displays the computer-generated time-domain formation in three different

configurations, (face-to-face (FF), face-to-side (FS), and side-to-side (SS)). In each of these configurations, two duplicate antennas are positioned 125 mm apart, or 2.5 times of the wavelength (λ_0) at 6 GHz. Single antenna serves as the transmitter (Tx) and the other as the reception one (Rx) in these arrangements. Figure 15 shows the group delay, S_{21} phases, and S_{21} magnitudes. In contrast, the FF and SF antenna designs have an S_{21} value below -40 dB at 4.5 GHz, lower than -50 at 6 GHz and 8 GHz. This is clearly shown in Figure 15(a), where the SS antenna design has an S_{21} value around -25 dB at 4.5 GHz and 6 GHz and rises to -32 dB at 8 GHz. To further appreciate the linearity features inside the planned band operation, Figure 15(b) also shows the S_{21} phase. The phase curves designate that the antenna displays linear activities inside the wanted frequency range crossways different placements. To support this finding, Figure 15(c) offers the group delay data. The group delay is roughly 0.1 ns at 4.5 GHz, and about 0.05 ns and 0.19 ns at 6 GHz and 8 GHz, respectively.
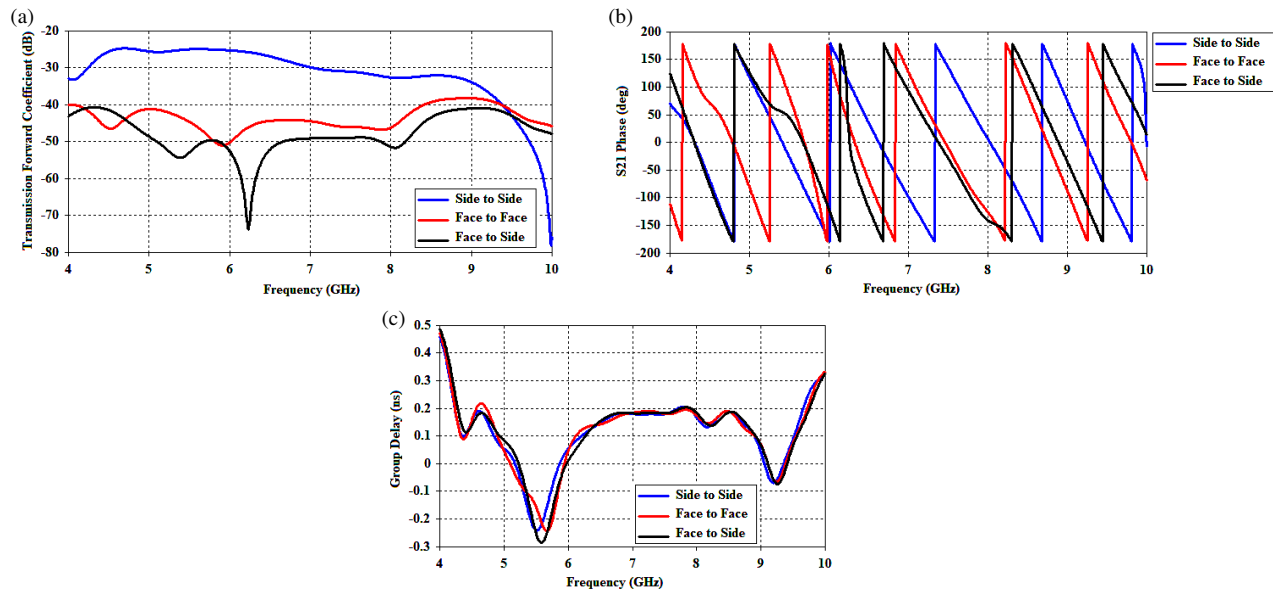
FIGURE 15. Performance analysis of the proposed antenna in the time domain. (a) Transmission forward coefficient, (b) S_{21} phase, and (c) group delay.
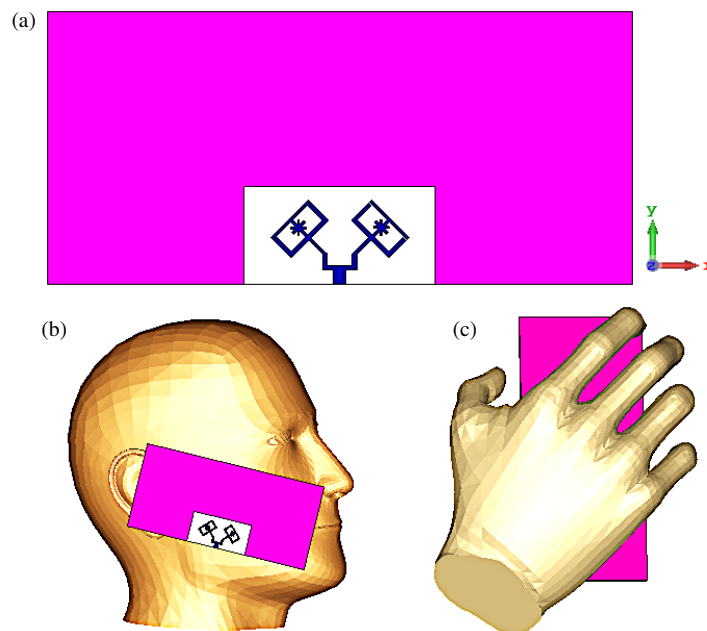

FIGURE 16. (a) Diagram of antenna with dielectric back cover; (b) antenna arrangement configuration using hand phantom model; and (c) Designed antenna with a HPM for SAR analysis.

5. FEATURES OF RADIATION AND THE INFLUENCE ON THE OPERATOR'S HAND AND HEAD

Specific absorption rate (SAR) is a statistic used to quantify the quantity of electromagnetic (EM) radiation that is engrossed by the human body when a mobile phone is used [33–37]. Since the proposed antenna array is attached to the rear cover, the SAR value must be predicted. The dielectric substance used to make this rear cover has a loss tangent of 0.002 and a permittivity of 3.32. The antenna arrangement on the rear cover, which measures $150 \times 70 \times 1.2\,\text{mm}^3$, is shown in Figure 16(a).

Since the planned antenna is meant to be used with mobile phones, it is imperative to estimate its SAR. As Figure 16(b) shows, the planning architecture is meant to judge the EM engrossed by the person's head using a human head phantom model (HPM). The antenna is positioned at a 65° angle with respect to the perpendicular axis that is negative. It is important to remember that, as discussed in [38], the departure space among the antenna element and various body components has a considerable impact on the SAR value. The simulation used in our work places the antenna array 5 mm from the HPM, more precisely, close to the mouth and ear areas.
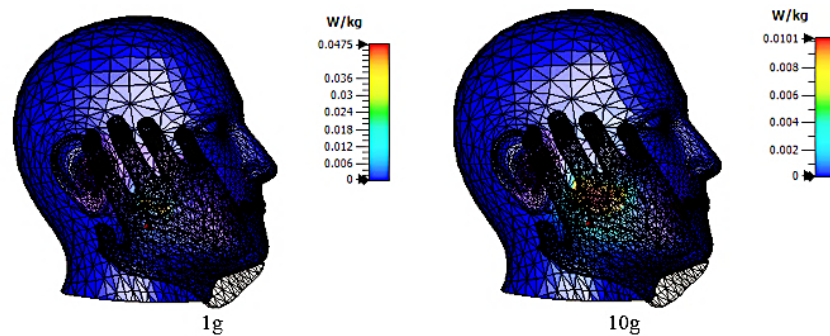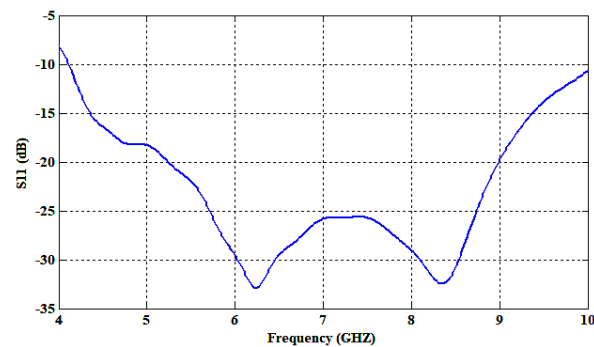
FIGURE 17. The results of SAR analysis at 4.5 GHz.

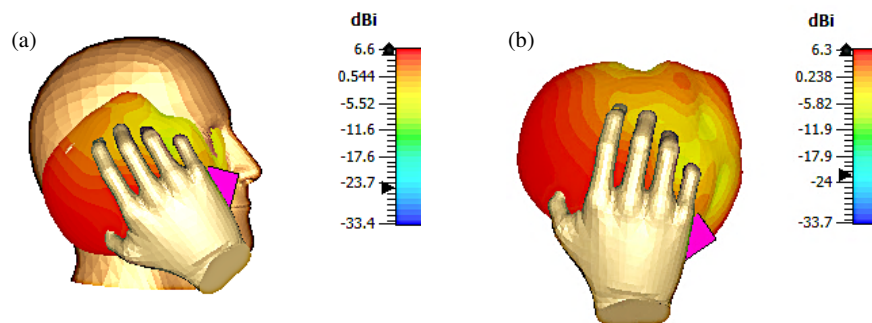FIGURE 18. S-parameter readings in data mode while the hand is present.

FIGURE 19. The effects of user hand and head movements on the recommended antenna array's 3D radiation characteristics at 4.5 GHz (a) talking mode, and (b) data mode.

The array antenna's setup is shown on a Single Hand Mode model (SHM) in Figure 16(c), which is intended to judge the antenna's functionality in data mode. The antenna is oriented in a way that maximizes user comfort in various settings. Specifically, there is a little space about 0.2 mm between the array antenna's ground plane and the HPM. The antenna's configuration is shown on an SHM model in Figure 16(c), which is intended to assess the antenna's functionality in data mode. The antenna is oriented and positioned in a way that maximizes user comfort in various settings. Specifically, there is a little distance of around 0.2 mm between the antenna's ground plane and the hand phantom model.

Figure 17 displays the SAR value obtained from simulations. It is imperative to note that the computer-generated SAR sprays inside the satisfactory range of conventional SAR values (1.6 W/kg). The influence of the operator's hand on the

antenna array is evaluated for sub-6 GHz 5G at the 4.5 GHz resonance frequency. Crucially, the antenna's effectiveness is greatly impacted by its placement above the hand. The simulation results for the proposed structure's $SAR_{1\,g}$ and $SAR_{10\,g}$ at 4.5 GHz with 15 dBm power are shown in Table 4. It is obvious that the $SAR_{10\,g}$ values at 4.5 GHz are comparable to 0.0101 W/kg, which is within permissible parameters and that all of the computer-generated values comply with the structural constraints set by the FCC and International Commission on Non-Ionizing Radiation Protection (ICNIRP) standards.

Figure 18 shows how the S-parameters have changed. It is found that announcing dielectric loading via the SHM leads to a lessening in impedance matching. Figure 19 illustrates the radiation patterns of the antenna once a head model, a hand model, and a rearmost antenna with a back cover are added to the setup.

TABLE 4. 15 dBm power simulations of the proposed structure's SAR_{1g} and SAR_{10g}.

	Distance 5 mm		Distance 10 mm	
Frequency	SAR_{1g} (W/kg)	SAR_{10g} (W/kg)	SAR_{1g} (W/kg)	SAR_{10g} (W/kg)
At 4.5 GHZ	0.0475	0.0101	0.0357	0.0095

TABLE 5. Detailed comparison of the planned antenna with the past work.

Ref	Size	Operating Band (GHz)	Covered wireless standards	Gain (dBi)	Efficiency	SAR
[9]	$0.46\lambda_0 \times 0.29\lambda_0$	2.3–3.0 3.25–3.68 4.9–6.2	WiMAX-WLAN-C band	4.32	NA	NA
[16]	$0.24\lambda_0 \times 0.18\lambda_0$	3.1–10.6	WiMAX-WLAN-X band	2.5	NA	NA
[17]	$0.38\lambda_0 \times 0.34\lambda_0$	2.34–2.82 3.16–4.06 4.695.37	WiMAX-WLAN	3.02	55%	NA
[22]	$0.9\lambda_0 \times 0.78\lambda_0$	2.75–5.45	WiMAX-WLAN	8.4	NA	NA
[24]	$0.39\lambda_0 \times 0.28\lambda_0$	3.5–3.75 4.85–5.2 5.5–5.7	WiMAX-WLAN-C band	8	40%	NA
[39]	$0.24\lambda_0 \times 0.19\lambda_0$	4.8–5.18 5.63–5.95 6.25–6.83	WiMAX-WLAN-C band	8	95%	NA
[40]	$0.62\lambda_0 \times 0.62\lambda_0$	1.09–2.08	5G NR-Wi-Fi-UMTS	8.1	80%	$SAR_{10g} =$ 0.007 (W/kg)
[41]	$0.82\lambda_0 \times 0.69\lambda_0$	4–6	WiMAX-WLAN-C band	8.2	NA	$SAR_{10g} =$ 0.1 (W/kg)
[42]	$0.3\lambda_0 \times 0.17\lambda_0$	3.29–3.63 4.39–5.2	WiMAX-WLAN-C band	7.17	92%	NA
[43]	$0.7\lambda_0 \times 0.7\lambda_0$	3–6	WiMAX-WLAN-C band	4	98%	$SAR_{10g} =$ 1.8 (W/kg)
[44]	$0.260\lambda_0 \times 0.25\lambda_0$	11.81/4.27/4.29/ 6.62/3.27/4.22/8.13	WiMAX-WLAN-KU-X band	4	80%	0.13
[45]	$0.4884\lambda_0 \times 0.4329\lambda_0$	5.11/7.33/11.70/ 6.38/12.03/5.62	WLAN-WiMAX-C-X-KU band	4	84%	NA
[46]	$0.299\lambda_0 \times 0.4385\lambda_0$	3.5/ 5/ 5.8	WLAN-WiMAX band	3.31	82.9%	NA
[47]	$0.7\lambda_0 \times 0.58\lambda_0$	28.48/11.32/41.33/ 26.82/6.76/8.50/11.79	WLANWiMAX-X-C-KU band	3.9	82%	NA
[48]	$0.55\lambda_0 \times 0.4\lambda_0$	2.42/4.34/5.81/8.45/ 11.02/13.98/16.12/18.87	S- C- X-Ku- K band	3.5	82%	NA
Proposed work	$0.8\lambda_0 \times 0.5\lambda_0$	4-more than 10	5G sub 6 GHz-WLAN-WiMAX-C-X band	11	95%	$SAR_{10g} =$ 0.0101 (W/kg) $SAR_{1g} =$ 0.0475 (W/kg)

Where λ_0 represents the free-space wavelength.

TABLE 6. SAR comparison among the planned scheme and past work.

Ref.	Distance (mm)	Power (dBm)	No. of ports	$SAR_{1\,g}$ (W/kg)	$SAR_{10\,g}$ (W/kg)
[49]	5	24	2	1.35	Non
[50]	Non	Non	Non	1.42	0.3
[51]	Non	24	8	Non	1.2
[52]	Non	Non	2	Non	0.37
Proposed work	5	15	1	0.0475	0.0101

6. COMPARISON WITH RELATED WORK

It is difficult to give up small dimensions for a wideband antenna with exceptional performance, despite efforts to create one with a low profile and high gain. This work presents a high-gain super-compact wideband antenna array with a semi-circular DGS for 5G smartphones and C-band application. The influence of human tissues and the dielectric back cover were studied since they are believed to be the most relevant in terms of mobile terminal applications. The suggested structure is created for 5G sub-6 GHz and C-band requests

The planned antenna shows exceptional characteristics and functionality with respect to size, operating band (GHz), and gain (dBi) compared to the works provided in the publications in Table 5. Table 5 lists the competing variants of the antenna designs that are available. These variations are displayed in the comparison. The findings clearly show that the planned antenna, which is appropriate for 5G terminal devices, is smaller than the reference antennas and has the highest gain. To make it easier to compare the SAR levels, Table 6 is added. Table 6 makes it evident that, in comparison to the SAR values reported in earlier studies, the finalized antenna array's results usually display a lower level.

7. CONCLUSION

In this study, we propose a high-gain, ultra-compact, and efficient wideband antenna array with a semicircular DGS-based metamaterial for 5G smartphones and C-band applications. Our design incorporates two orthogonal antennas to enhance the gain. Simulations were conducted using CST software to optimize the size of the antenna elements. The proposed antenna array achieves a high efficiency of 95% and operates in the frequency range of 4 GHz to over 10 GHz, with peak gain values reaching 11 dBi across this range. A thorough time-domain analysis was conducted to validate the radiation efficiency of the antenna array. Additionally, SAR analysis confirms that the array is suitable for 5G mobile devices operating within the target frequency range. The simulated and experimental results show excellent agreement. This study's future is broad and bright, propelled by developments in wireless communication, new applications, and the increasing need for dependable, fast connectivity. Important fields are as follows in which antenna technology will be crucial: beamforming, smart antennas, and massive MIMO.

REFERENCES

[1] Thakur, E., A. Gupta, M. K. Abdulhameed, A. D. Khaleel, and A. J. A. Al-Gburi, "Microstrip antenna with two elements and defected ground structure for 5G mobile applications at 28/38 GHz," *Progress In Electromagnetics Research C*, Vol. 146, 177–185, 2024.

[2] Bose, M. and V. Karuppiah, "Metamaterial inspired superstrate loaded miniaturized quad port MIMO antenna for 5G C-band applications," *Optics Communications*, Vol. 574, 131123, 2025.

[3] Kumar, P., A. K. Singh, R. Kumar, S. K. Mahto, P. Pal, R. Sinha, A. Choubey, and A. J. A. Al-Gburi, "Design and analysis of low profile stepped feedline with dual circular patch MIMO antenna and stub loaded partial ground plane for wireless applications," *Progress In Electromagnetics Research C*, Vol. 140, 135–144, 2024.

[4] Elabd, R. H. and A. A. Megahed, "Isolation enhancement of a two-orthogonal printed elliptical slot MIMO antenna array with EBG structure for millimeter wave 5G applications," *Discover Applied Sciences*, Vol. 6, No. 5, 222, 2024.

[5] Lak, A., Z. Adelpour, H. Oraizi, and N. Parhizgar, "Design and SAR assessment of three compact 5G antenna arrays," *Scientific Reports*, Vol. 11, No. 1, 21265, 2021.

[6] Asif, S. M., M. R. Anbiyaei, K. L. Ford, T. O'Farrell, and R. J. Langley, "Low-profile independently-and concurrently-tunable quad-band antenna for single chain sub-6 GHz 5G new radio applications," *IEEE Access*, Vol. 7, 183 770–183 782, 2019.

[7] Sarkar, D. and K. V. Srivastava, "Four element dual-band sub-6 GHz 5G MIMO antenna using SRR-loaded slot-loops," in *2018 5th IEEE Uttar Pradesh Section International Conference on Electrical, Electronics and Computer Engineering (UPCON)*, 1–5, Gorakhpur, India, 2018.

[8] Wang, T., G. Li, J. Ding, Q. Miao, J. Li, and Y. Wang, "5G spectrum: Is China ready?" *IEEE Communications Magazine*, Vol. 53, No. 7, 58–65, 2015.

[9] Dang, L., Z. Y. Lei, Y. J. Xie, G. L. Ning, and J. Fan, "A compact microstrip slot triple-band antenna for WLAN/WiMAX applications," *IEEE Antennas and Wireless Propagation Letters*, Vol. 9, 1178–1181, 2010.

[10] Marzouk, M., I. H. Nejdi, R. Youssef, S. Barua, S. Mohamed, S. Ahmad, and M. Hussein, "Efficient broadband fractal antenna for WiMAX and WLAN," *Heliyon*, Vol. 10, No. 5, 1–13, 2024.

[11] Mohanraj, P. and P. R. Selvakumaran, "Compact wideband implantable antenna for biomedical applications," *Current Applied Physics*, Vol. 43, 50–56, 2022.

[12] Lamminen, A., J. Säily, J. Ala-Laurinaho, J. de Cos, and V. Ermolov, "Patch antenna and antenna array on multilayer high-frequency PCB for D-band," *IEEE Open Journal of Antennas and Propagation*, Vol. 1, 396–403, 2020.

[13] Zheng, Q., J. Ma, Z. Wu, and P. PourMohammadi, "Dual-broadband high-isolation circularly polarized Low-RCS shared-aperture antenna array based on mushroom-type metasurface," *Optics Communications*, Vol. 574, 131127, 2025.

[14] Zhou, Z., Z. Wei, Z. Tang, and Y. Yin, "Design and analysis of a wideband multiple-microstrip dipole antenna with high isolation," *IEEE Antennas and Wireless Propagation Letters*, Vol. 18, No. 4, 722–726, 2019.

[15] Liu, Y., X. Li, L. Yang, and Y. Liu, "A dual-polarized dual-band antenna with omni-directional radiation patterns," *IEEE Transactions on Antennas and Propagation*, Vol. 65, No. 8, 4259–4262, 2017.

[16] Bod, M., H. R. Hassani, and M. M. S. Taheri, "Compact UWB printed slot antenna with extra bluetooth, GSM, and GPS bands," *IEEE Antennas and Wireless Propagation Letters*, Vol. 11, 531–534, 2012.

[17] Hu, W., Y.-Z. Yin, P. Fei, and X. Yang, "Compact triband square-slot antenna with symmetrical L-strips for WLAN/WiMAX applications," *IEEE Antennas and Wireless Propagation Letters*, Vol. 10, 462–465, 2011.

[18] Li, M.-Y., Y.-L. Ban, Z.-Q. Xu, G. Wu, C.-Y.-D. Sim, K. Kang, and Z.-F. Yu, "Eight-port orthogonally dual-polarized antenna array for 5G smartphone applications," *IEEE Transactions on Antennas and Propagation*, Vol. 64, No. 9, 3820–3830, 2016.

[19] Dong, X., Z. Liao, J. Xu, Q. Cai, and G. Liu, "Multiband and wideband planar antenna for WLAN and WiMAX applications," *Progress In Electromagnetics Research Letters*, Vol. 46, 101–106, 2014.

[20] Xiong, L. and P. Gao, "Compact dual-band printed diversity antenna for WIMAX/WLAN applications," *Progress In Electromagnetics Research C*, Vol. 32, 151–165, 2012.

[21] Mok, W. C., S. H. Wong, K. M. Luk, and K. F. Lee, "Single-layer single-patch dual-band and triple-band patch antennas," *IEEE Transactions on Antennas and Propagation*, Vol. 61, No. 8, 4341–4344, 2013.

[22] Pandeeswari, R., "Complimentary split ring resonator inspired meandered CPW-fed monopole antenna for multiband operation," *Progress In Electromagnetics Research C*, Vol. 80, 13–20, 2018.

[23] Alsaif, H., M. Usman, M. T. Chughtai, and J. Nasir, "Cross polarized 2 × 2 UWB-MIMO antenna system for 5G wireless applications," *Progress In Electromagnetics Research M*, Vol. 76, 157–166, 2018.

[24] Lee, K.-F., S. L. S. Yang, and A. A. Kishk, "Dual-and multiband U-slot patch antennas," *IEEE Antennas and Wireless Propagation Letters*, Vol. 7, 645–647, 2008.

[25] Barani, I. R. R., K.-L. Wong, Y.-X. Zhang, and W.-Y. Li, "Low-profile wideband conjoined open-slot antennas fed by grounded coplanar waveguides for 4 × 4 5G MIMO operation," *IEEE Transactions on Antennas and Propagation*, Vol. 68, No. 4, 2646–2657, 2020.

[26] ANSI, , "Safety levels with respect to human exposure to radio-frequency electromagnetic fields, 3 kHz-300 GHz," *IEEE Std C.*, Vol. 95, No. 1, 2006.

[27] Ahlbom, A., U. Bergqvist, J. H. Bernhardt, J. P. Cesarini, M. Grandolfo, M. Hietanen, A. F. Mckinlay, M. H. Repacholi, D. H. Sliney, *et al.*, "Guidelines for limiting exposure to time-varying electric, magnetic, and electromagnetic fields (up to 300 GHz)," *Health Physics*, Vol. 74, No. 4, 494–521, 1998.

[28] Liu, N.-W., L. Zhu, W.-W. Choi, and J.-D. Zhang, "A low-profile differentially fed microstrip patch antenna with broad impedance bandwidth under triple-mode resonance," *IEEE Antennas and Wireless Propagation Letters*, Vol. 17, No. 8, 1478–1482, 2018.

[29] Elabd, R. H. and A. J. A. Al-Gburi, "SAR assessment of miniaturized wideband MIMO antenna structure for millimeter wave 5G smartphones," *Microelectronic Engineering*, Vol. 282, 112098, 2023.

[30] Elabd, R. H. and A. J. A. Al-Gburi, "Super-compact 28/38 GHz 4-port MIMO antenna using metamaterial-inspired EBG structure with SAR analysis for 5G cellular devices," *Journal of Infrared, Millimeter, and Terahertz Waves*, Vol. 45, No. 1, 35–65, 2024.

[31] Gómez, L. and A. S. Ibrahim, "Design, analysis and simulation of microstrip antenna arrays with flexible substrate in different frequency, for use in UAV-assisted marine communications," *Journal of Marine Science and Engineering*, Vol. 11, No. 4, 730, 2023.

[32] Sediq, H. T., J. Nourinia, and C. Ghobadi, "A cat-shaped patch antenna for future super wideband wireless microwave applications," *Wireless Personal Communications*, Vol. 125, No. 2, 1307–1333, 2022.

[33] Lak, A., Z. Adelpour, H. Oraizi, and N. Parhizgar, "Design and SAR assessment of three compact 5G antenna arrays," *Scientific Reports*, Vol. 11, No. 1, 21265, 2021.

[34] Al-Gburi, A. J. A., M. M. Ismail, N. J. Mohammed, and T. A. H. Alghamdi, "SAR flexible antenna advancements: Highly conductive polymer-graphene oxide-silver nanocomposites," *Progress In Electromagnetics Research M*, Vol. 127, 23–30, 2024.

[35] Zada, M., I. A. Shah, and H. Yoo, "Integration of sub-6-GHz and mm-wave bands with a large frequency ratio for future 5G MIMO applications," *IEEE Access*, Vol. 9, 11 241–11 251, 2021.

[36] Elabd, R. H. and A. J. A. Al-Gburi, "Ultra-compact 4-port MIMO antenna with defected ground structure and SAR analysis for 28/38 GHz 5G mobile devices," *Journal of Electromagnetic Waves and Applications*, Vol. 38, No. 9, 1000–1025, 2024.

[37] Elabd, R. H. and A. J. A. Al-Gburi, "Low mutual coupling miniaturized dual-band quad-port MIMO antenna array using decoupling structure for 5G smartphones," *Discover Applied Sciences*, Vol. 6, No. 4, 189, 2024.

[38] Abdullah Al-Gburi, A. J., "5G MIMO antenna: Compact design at 28/38 GHz with metamaterial and SAR analysis for mobile phones," *Przegląd Elektrotechniczny*, Vol. 2024, No. 4, 171–174, 2024.

[39] Xue, Q., S. W. Liao, and J. H. Xu, "A differentially-driven dual-polarized magneto-electric dipole antenna," *IEEE Transactions on Antennas and Propagation*, Vol. 61, No. 1, 425–430, 2013.

[40] Pan, Y. M., P. F. Hu, X. Y. Zhang, and S. Y. Zheng, "A low-profile high-gain and wideband filtering antenna with metasurface," *IEEE Transactions on Antennas and Propagation*, Vol. 64, No. 5, 2010–2016, 2016.

[41] Ishteyaq, I., I. S. Masoodi, and K. Muzaffar, "A compact double-band planar printed slot antenna for sub-6 GHz 5G wireless applications," *International Journal of Microwave and Wireless Technologies*, Vol. 13, No. 5, 469–477, 2021.

[42] Parsa, J. and A. Webb, "Specific absorption rate (SAR) simulations for low-field ($< 0.1\,$T) MRI systems," *Magnetic Resonance Materials in Physics, Biology and Medicine*, Vol. 36, No. 3, 429–438, 2023.

[43] Megahed, A. A., M. Abdelazim, E. H. Abdelhay, and H. Y. M. Soliman, "Sub-6 GHz highly isolated wideband MIMO antenna arrays," *IEEE Access*, Vol. 10, 19 875–19 889, 2022.

[44] Saraswat, R. K. and M. Kumar, "A metamaterial hepta-band antenna for wireless applications with specific absorption rate reduction," *International Journal of RF and Microwave Computer-Aided Engineering*, Vol. 29, No. 10, e21824, 2019.

[45] Saraswat, R. K. and M. Kumar, "A vertex-fed hexa-band frequency reconfigurable antenna for wireless applications," *International Journal of RF and Microwave Computer-Aided Engineering*, Vol. 29, No. 10, e21893, 2019.

[46] Saraswat, R. K. and M. Kumar, "Implementation of metamaterial loading to miniaturized UWB dipole antenna for WLAN and WiMAX applications with tunability characteristics," *IETE Journal of Research*, Vol. 68, No. 3, 2022–2035, 2022.

[47] Saraswat, R. K. and M. Kumar, "Implementation of hybrid fractal metamaterial inspired frequency band reconfigurable multi-band antenna for wireless applications," *International Journal of RF and Microwave Computer-Aided Engineering*, Vol. 30, No. 9, e22315, 2020.

[48] Saraswat, R. K. and M. Kumar, "Implementation of the metamaterial multiband frequency reconfigurable antenna for IoT wireless standards," *IETE Journal of Research*, Vol. 70, No. 5, 4594–4605, 2024.

[49] Zada, M., I. A. Shah, and H. Yoo, "Integration of sub-6-GHz and mm-wave bands with a large frequency ratio for future 5G MIMO applications," *IEEE Access*, Vol. 9, 11 241–11 251, 2021.

[50] Ojaroudi Parchin, N., M. Alibakhshikenari, H. J. Basherlou, R. A. Abd-Alhameed, J. Rodriguez, and E. Limiti, "MM-wave phased array Quasi-Yagi antenna for the upcoming 5G cellular communications," *Applied Sciences*, Vol. 9, No. 5, 978, 2019.

[51] Khan, J., D. A. Sehrai, and U. Ali, "Design of dual band 5G antenna array with SAR analysis for future mobile handsets," *Journal of Electrical Engineering & Technology*, Vol. 14, 809–816, 2019.

[52] Lak, A., Z. Adelpour, H. Oraizi, and N. Parhizgar, "Design and SAR assessment of three compact 5G antenna arrays," *Scientific Reports*, Vol. 11, No. 1, 21265, 2021.